AGU PUBLICATIONS

JGR

Journal of Geophysical Research: Space Physics

RESEARCH ARTICLE
10.1002/2016JA022827

Special Section:
Measurement Techniques in Solar and Space Physics: Fields

Revised single-spacecraft method for determining wave vector k and resolving space-time ambiguity

P. M. Bellan[1]

[1] Applied Physics and Materials Science, Caltech, Pasadena, California, USA

Key Points:
- I present a method for measuring wave vector using a single spacecraft
- The method resolves space-time ambiguity of single space-craft measurements
- The plasma-frame wave frequency can be deduced from a moving spacecraft

Supporting Information:
- Supporting Information S1

Correspondence to:
P. M. Bellan,
pbellan@its.caltech.edu

Citation:
Bellan, P. M. (2016), Revised single-spacecraft method for determining wave vector **k** and resolving space-time ambiguity, *J. Geophys. Res. Space Physics*, *121*, 8589–8599, doi:10.1002/2016JA022827.

Received 19 APR 2016
Accepted 30 AUG 2016
Accepted article online 7 SEP 2016
Published online 22 SEP 2016

Abstract A practical method is proposed for determining the wave vector of waves from single-spacecraft measurements. This wave vector knowledge can then be used to remove the space-time ambiguity produced by frequency Doppler shift associated with spacecraft motion. The method involves applying the Wiener-Khinchin theorem to cross correlations of the current and magnetic field oscillations and to autocorrelations of the magnetic field oscillations. The method requires that each wave frequency component map to a unique wave vector, a condition presumed true in many spacecraft measurement situations. Examples validating the method are presented.

1. Introduction

The determination of the magnitude and direction of the wave vector **k** from single spacecraft measurements has long been a challenge to space physicists. Closely associated with this issue has been the space-time ambiguity where it is unclear whether a temporal fluctuation measured in the spacecraft frame results from a temporal fluctuation in the plasma frame or instead from the spacecraft flying through a spatially dependent structure that is stationary in the plasma frame. The most widely used previous methods to determine the direction and magnitude of **k** are the minimum-variance method, the phase-difference determination, and the multispacecraft k-filtering method [*Sonnerup and Scheible*, 1998; *Motschmann and Glassmeier*, 1998; *Balikhin et al.*, 2003; *Narita et al.*, 2010]. However, some of these methods only resolve the direction relative to the background magnetic field within a sign ambiguity along the field, while others require a wave dispersion relation from a model to resolve the wave vector **k**.

Bellan [2012] proposed that if the wave electric current density **J** has zero divergence as is true for low-frequency waves such as Alfvén or ion-cyclotron waves, then knowledge of **J** could provide a means for resolving both **k** and the space-time ambiguity inherent in single-spacecraft measurements. Intuitively, this is because $\mu_0\mathbf{J} = i\mathbf{k}\times\mathbf{B}$ implies that knowledge of **J** and of the wave magnetic field **B** should suffice to determine **k**, the only issue being that $\mu_0\mathbf{J} = i\mathbf{k}\times\mathbf{B}$ contains no information about the component of **k** parallel to **B**. However, this issue is resolved because $\nabla\cdot\mathbf{B} = 0$ implies that **k** has no component parallel to **B**.

We note that *Santolik et al.* [2003] discussed a singular value decomposition technique for determining the wave vector of *high-frequency* waves using information from the wave electric field **E** and magnetic field **B**. Their method involved two steps: (i) the direction of **k** was determined using the orthogonality of **k** to both **B** and its complex conjugate $\mathbf{B}^*$ and then (ii) the magnitude $|\mathbf{k}|$ was determined using Faraday's law $\mathbf{k}\times\mathbf{E} = \omega\mathbf{B}$.

The low-frequency method proposed by *Bellan* [2012] for resolving **k** differed from that proposed in *Korepanov and Dudkin* [1999] by taking into account the divergence-free nature of **B** and, for low-frequencies, of **J**. The method in *Bellan* [2012] was a by-product of the identification in *Bellan* [2012] that if a plasma wave is quasi-neutral, there are advantages in using the wave current **J** as the fundamental quantity rather than the more commonly used wave electric field **E**. In particular, the wave dispersion derived using **J** involved the trivial task of evaluating the determinant of a 2×2 matrix, whereas derivation of the same dispersion using **E** required the very nontrivial task of evaluating the determinant of a fully populated 3×3 matrix.

Measuring **J** has generally not been feasible in older spacecraft because plasma electrons and ions were sampled at a much slower cadence than electric and magnetic field measurements. Even worse, there was typically substantial time-resolution difference between ion and electron measurements so that determination of **J** was uncertain at any time scale. However, modern missions such as the Magnetospheric Multiscale Mission have high-cadence measurements of particle fluxes and so now offer the opportunity to carry out fast and

comparable plasma (electrons and ions) and field (electric and magnetic) measurements. Thus, it should now be possible to resolve **J** and so obtain **k** from single-spacecraft measurements for low-frequency quasi-neutral waves. Because of particle detector frequency response limitations, the method is expected to be limited to frequencies of order 10–20 Hz for the present.

2. Identification of Shortcoming in Previous Method [*Bellan*, 2012]

The purpose of this paper is to identify a shortcoming in the method given in *Bellan* [2012] and present a revised method that overcomes this shortcoming. In *Bellan* [2012] it was argued that **k** must be orthogonal to both **B** and **J** because $\mathbf{k}\cdot\mathbf{B}=0$ and $\mathbf{k}\cdot\mathbf{J}=0$ and so **k** should be normal to the plane in which **B** and **J** lie. Thus, it was argued that **k** should be parallel to $\mathbf{B}\times\mathbf{J}$. However, a recent attempt [A. F. Viñas, private communication, 2016] to implement this procedure revealed ambiguities because **B** and **J** are complex Fourier-space quantities and their cross product is also complex, whereas **k** is a real vector. In attempting to address this issue, an additional problem was identified, namely, **B** and **J** are not orthogonal if the wave is circularly polarized. To see this, consider the circularly polarized wave

$$\mathbf{B}(z,t)=b\left(\hat{x}+i\hat{y}\right)e^{i(k_z z-\omega t)} \tag{1}$$

which has an associated current density

$$\begin{aligned}\mathbf{J}&=\mu_0^{-1}\nabla\times\mathbf{B}\\&=\mu_0^{-1}k_z b\left(\hat{x}+i\hat{y}\right)e^{i(k_z z-\omega t)}\end{aligned} \tag{2}$$

so **J** is parallel to **B** in which case $\mathbf{B}\times\mathbf{J}$ vanishes. However, if one were to calculate $\mathbf{B}\times\mathbf{J}^*$, then one finds

$$\begin{aligned}\mathbf{B}\times\mathbf{J}^*&=\left[b\left(\hat{x}+i\hat{y}\right)e^{i(kz-\omega t)}\right]\times\left[\mu_0^{-1}k_z b^*\left(\hat{x}-i\hat{y}\right)e^{-i(k_z z-\omega t)}\right]\\&=-2ik_z\mu_0^{-1}\left|b\right|^2\hat{z}\end{aligned} \tag{3}$$

which is proportional to k_z and in the z direction, i.e., is parallel to **k**.

3. Revised Method

The above result motivates the following general procedure which should be feasible to implement for actual spacecraft measurements. In order to minimize notational clutter, Fourier transforms and real-space quantities from now on will be identified by their argument so, for example, $\psi(\omega)$ denotes the temporal Fourier transform of $\psi(t)$. The time-dependent magnetic field and current density at some position **x** can be expressed as a sum of waves:

$$\mathbf{B}(\mathbf{x},t)=\int_{-\infty}^{\infty}\mathrm{d}\omega\mathbf{B}(\omega)e^{i\mathbf{k}(\omega)\cdot x-i\omega t} \tag{4}$$

$$\mathbf{J}(\mathbf{x},t)=\int_{-\infty}^{\infty}\mathrm{d}\omega\mathbf{J}(\omega)e^{i\mathbf{k}(\omega)\cdot x-i\omega t} \tag{5}$$

where $\mathbf{k}(\omega)$ is determined by the relevant wave dispersion relation. If there are only quasi-neutral traveling waves and no standing waves, Ampere's law assumes the form

$$\mu_0\mathbf{J}(\omega)=i\mathbf{k}(\omega)\times\mathbf{B}(\omega). \tag{6}$$

The requirement of no standing waves provides a unique **k** for each ω and so prevents the ambiguous situation where in addition to having a particular **k** for some ω there is also a $-\mathbf{k}$; this and related caveats are discussed in detail in section 6. This assumption of a unique **k** for each ω has been successfully used in many actual space physics situations [*Balikhin et al.*, 2003; *Hobara et al.*, 2007; *Volwerk et al.*, 2008; *Walker et al.*, 2015] and is presumed to correspond to observation of waves generated by a single localized distant source. The omission of displacement current in equation (6) corresponds to the quasi-neutrality assumption; this assumption is associated with the wave phase velocity being negligible compared to the speed of light so that displacement current can be dropped from Ampere's law.

Crossing equation (6) with $\mathbf{B}^*(\omega)$ and using $\mathbf{k}\cdot\mathbf{B}(\omega)=0$ gives

$$\begin{aligned}\mu_0\mathbf{J}(\omega)\times\mathbf{B}^*(\omega) &= (i\mathbf{k}(\omega)\times\mathbf{B}(\omega))\times\mathbf{B}^*(\omega) = \mathbf{B}(\omega)i\mathbf{k}(\omega)\cdot\mathbf{B}^*(\omega) - i\mathbf{k}(\omega)\mathbf{B}(\omega)\cdot\mathbf{B}^*(\omega)\\ &= \mathbf{B}(\omega)i\left[\mathbf{k}(\omega)\cdot\mathbf{B}(\omega)\right]^* - i\mathbf{k}(\omega)\mathbf{B}(\omega)\cdot\mathbf{B}^*(\omega) = -i\mathbf{k}(\omega)\mathbf{B}(\omega)\cdot\mathbf{B}^*(\omega)\end{aligned} \tag{7}$$

so

$$\mathbf{k}(\omega) = i\mu_0\frac{\mathbf{J}(\omega)\times\mathbf{B}^*(\omega)}{\mathbf{B}(\omega)\cdot\mathbf{B}^*(\omega)} \tag{8}$$

which is our main result.

This result can be expressed in another equivalent way which might be more practical to use. Consider the complex conjugate of equation (4)

$$\mathbf{B}(\mathbf{x},t) = \int_{-\infty}^{\infty} d\omega\mathbf{B}^*(\omega)e^{-i\mathbf{k}(\omega)\cdot\mathbf{x}+i\omega t} \tag{9}$$

where the left-hand side remains the same because $\mathbf{B}(\mathbf{x},t)$ is a real quantity. Letting $\omega\to-\omega$, this becomes

$$\mathbf{B}(\mathbf{x},t) = \int_{-\infty}^{\infty} d\omega\mathbf{B}^*(-\omega)e^{-i\mathbf{k}(-\omega)\cdot\mathbf{x}-i\omega t} \tag{10}$$

which upon comparison with equation (4) gives the reality conditions [*Bernstein and Engelmann*, 1966; *Schmidt*, 1979; *P. M. Bellan*, 2008]

$$\mathbf{B}^*(-\omega) = \mathbf{B}(\omega) \tag{11}$$

$$\mathbf{k}(-\omega) = -\mathbf{k}(\omega). \tag{12}$$

We now define the spacecraft position to be $\mathbf{x}=0$ and let angle brackets denote time average of a quantity over a time duration T. Thus, using equations 4 and 5, the time average of $\mathbf{J}(t)\times\mathbf{B}(t)$ is

$$\langle\mathbf{J}(t)\times\mathbf{B}(t)\rangle = \frac{1}{T}\int_0^T dt\left(\left[\int_{-\infty}^{\infty} d\omega\mathbf{J}(\omega)e^{-i\omega t}\right]\times\left[\int_{-\infty}^{\infty} d\omega'\mathbf{B}(\omega')e^{-i\omega' t}\right]\right). \tag{13}$$

On interchanging the order of integration and using

$$\delta(\omega+\omega') = \frac{1}{2\pi}\int_0^T dt e^{-i(\omega+\omega')t}, \tag{14}$$

equation (13) becomes

$$\begin{aligned}\langle\mathbf{J}(t)\times\mathbf{B}(t)\rangle &= \frac{1}{T}\int_{-\infty}^{\infty} d\omega\int_{-\infty}^{\infty} d\omega'\left(\mathbf{J}(\omega)\times\mathbf{B}(\omega')\right)\int_0^T dt e^{-i(\omega+\omega')t}\\ &= \frac{2\pi}{T}\int_{-\infty}^{\infty} d\omega\int_{-\infty}^{\infty} d\omega'\left(\mathbf{J}(\omega)\times\mathbf{B}(\omega')\right)\delta(\omega+\omega')\\ &= \frac{2\pi}{T}\int d\omega\mathbf{J}(\omega)\times\mathbf{B}(-\omega) = \frac{2\pi}{T}\int d\omega\mathbf{J}(\omega)\times\mathbf{B}^*(\omega).\end{aligned} \tag{15}$$

Using equation (6), this becomes

$$\begin{aligned}\langle\mathbf{J}(t)\times\mathbf{B}(t)\rangle &= \frac{2\pi}{\mu_0 T}\int d\omega\left[i\mathbf{k}(\omega)\times\mathbf{B}(\omega)\right]\times\mathbf{B}^*(\omega) = \frac{2\pi i}{\mu_0 T}\int d\omega\left(\mathbf{B}(\omega)\mathbf{k}(\omega)\cdot\mathbf{B}^*(\omega) - \mathbf{k}|B|^2\right)\\ &= -\frac{2\pi i}{\mu_0 T}\int d\omega\,\mathbf{k}(\omega)|\mathbf{B}(\omega)|^2 = \int d\omega\mathbf{G}(\omega)\end{aligned} \tag{16}$$

where

$$\mathbf{G}(\omega) = -\frac{2\pi i}{\mu_0 T}\mathbf{k}(\omega)|\mathbf{B}(\omega)|^2 \tag{17}$$

is similar to a spectral energy, but unlike a spectral energy is an odd function of ω. Because $\mathbf{k}(\omega)$ is an odd function of ω, it is seen that $\langle\mathbf{J}(t)\times\mathbf{B}(t)\rangle = 0$.

Let us now calculate the time average of $\mathbf{B}(t)\cdot\mathbf{B}(t)$, using the same method as in equation (15), i.e.,

$$\begin{aligned}\langle \mathbf{B}(t)\cdot\mathbf{B}(t)\rangle &= \frac{2\pi}{T}\int_{-\infty}^{\infty} d\omega \int_{-\infty}^{\infty} d\omega' \left(\mathbf{B}(\omega)\cdot\mathbf{B}(\omega')\right)\delta(\omega+\omega') = \frac{2\pi}{T}\int d\omega \mathbf{B}(\omega)\cdot\mathbf{B}(-\omega)\\ &= \frac{2\pi}{T}\int d\omega\,|\mathbf{B}(\omega)|^2 = \int d\omega S(\omega).\end{aligned} \tag{18}$$

where

$$S(\omega) = \frac{2\pi}{T}\,|\mathbf{B}(\omega)|^2 \tag{19}$$

is the spectral power density of the magnetic oscillations. Combination of equations (17) and (19) then gives

$$-i\mathbf{k}(\omega) = \frac{\mu_0\mathbf{G}(\omega)}{S(\omega)}. \tag{20}$$

The spectral density functions $\mathbf{G}(\omega)$ and $S(\omega)$ can be calculated in terms of auto and cross correlations using a variation of the Wiener-Khinchin theorem. Consider

$$\begin{aligned}F(\tau) = \langle \mathbf{B}(t)\cdot\mathbf{B}(t+\tau)\rangle &= \frac{1}{T}\int_0^T dt\left(\left[\int_{-\infty}^{\infty} d\omega \mathbf{B}(\omega)e^{-i\omega t}\right]\cdot\left[\int_{-\infty}^{\infty} d\omega' \mathbf{B}(\omega')e^{-i\omega'(t+\tau)}\right]\right)\\ &= \frac{1}{T}\int_{-\infty}^{\infty} d\omega \int_{-\infty}^{\infty} d\omega' \int_0^T dt\left(\mathbf{B}(\omega)\cdot\mathbf{B}(\omega')e^{-i(\omega+\omega')t-i\omega'\tau}\right)\\ &= \frac{2\pi}{T}\int_{-\infty}^{\infty} d\omega \int_{-\infty}^{\infty} d\omega'\,\delta(\omega+\omega')\left(\mathbf{B}(\omega)\cdot\mathbf{B}(\omega')e^{-i\omega'\tau}\right)\\ &= \frac{2\pi}{T}\int_{-\infty}^{\infty} d\omega\left(\mathbf{B}(\omega)\cdot\mathbf{B}(-\omega)e^{i\omega\tau}\right) = \frac{2\pi}{T}\int_{-\infty}^{\infty} d\omega\,\mathbf{B}(\omega)\,\cdot\,\mathbf{B}^*(\omega)e^{i\omega\tau}\\ &= \frac{2\pi}{T}\int_{-\infty}^{\infty} d\omega\;|\mathbf{B}(\omega)|^2\,e^{i\omega\tau}.\end{aligned} \tag{21}$$

We define a Fourier-like transform of $F(\tau)$ to be

$$\begin{aligned}F(\omega) = \frac{T}{4\pi^2}\int_0^T F(\tau)e^{-i\omega\tau}d\tau &= \frac{T}{4\pi^2}\int_0^T\left\{\frac{2\pi}{T}\int_{-\infty}^{\infty} d\omega'\;\left|\mathbf{B}(\omega')\right|^2 e^{i\omega'\tau}\right\}e^{-i\omega\tau}d\tau\\ &= \frac{T}{4\pi^2}\,\frac{2\pi}{T}\int_{-\infty}^{\infty} d\omega'\;\left|\mathbf{B}(\omega')\right|^2 2\pi\delta(\omega'-\omega) = \int_{-\infty}^{\infty} d\omega'\;\left|\mathbf{B}(\omega')\right|^2\;\delta(\omega'-\omega) = \;|\mathbf{B}(\omega)|^2\end{aligned} \tag{22}$$

and so $|\mathbf{B}(\omega)|^2$ is determined from the Fourier-like transform of $F(\tau)$, the autocorrelation function for the magnetic oscillation.

We similarly define the cross-correlation function

$$\begin{aligned}\mathbf{H}(\tau) = \langle \mathbf{J}(t)\times\mathbf{B}(t+\tau)\rangle &= \frac{1}{T}\int_{-\infty}^{\infty} d\omega \int_{-\infty}^{\infty} d\omega'\left(\mathbf{J}(\omega)\times\mathbf{B}(\omega')\right)\int_0^T dt e^{-i(\omega+\omega')t-i\omega'\tau}\\ &= \frac{2\pi}{T}\int_{-\infty}^{\infty} d\omega \int_{-\infty}^{\infty} d\omega'\left(\mathbf{J}(\omega)\times\mathbf{B}(\omega')\right)\delta(\omega+\omega')\,e^{-i\omega'\tau} = \frac{2\pi}{T}\int_{-\infty}^{\infty} d\omega\left(\mathbf{J}(\omega)\times\mathbf{B}(-\omega)\right)\,e^{i\omega\tau}\\ &= \frac{2\pi}{\mu_0 T}\int_{-\infty}^{\infty} d\omega\left\{\left[(i\mathbf{k}(\omega)\times\mathbf{B}(\omega))\right]\times\mathbf{B}^*(\omega)\right\}\,e^{i\omega\tau} = -\frac{2\pi i}{\mu_0 T}\int_{-\infty}^{\infty} d\omega\mathbf{k}(\omega)\,|\mathbf{B}(\omega)|^2\,e^{i\omega\tau}\end{aligned} \tag{23}$$

which has the corresponding Fourier-like transform

$$\begin{aligned}\mathbf{H}(\omega) = \frac{T}{4\pi^2}\int_0^T \mathbf{H}(\tau)e^{-i\omega\tau}d\tau &= \frac{T}{4\pi^2}\int_0^T\left\{-\frac{2\pi i}{\mu_0 T}\int_{-\infty}^{\infty} d\omega'\mathbf{k}(\omega')\left|\mathbf{B}(\omega')\right|^2\,e^{i\omega'\tau}\right\}e^{-i\omega\tau}d\tau\\ &= -\frac{i}{\mu_0}\int_{-\infty}^{\infty} d\omega'\mathbf{k}(\omega')\left|\mathbf{B}(\omega')\right|^2\,\delta(\omega'-\omega) = -\frac{i}{\mu_0}\mathbf{k}(\omega)\,|\mathbf{B}(\omega)|^2\,.\end{aligned} \tag{24}$$

Thus,

$$\mathbf{k}(\omega) = i\mu_0 \frac{\mathbf{H}(\omega)}{F(\omega)} \tag{25}$$

where $F(\omega)$ and $\mathbf{H}(\omega)$ are given by the first lines of equations (22) and (24), respectively. As in *Bellan* [2012], the plasma-frame frequency ω can be determined from the spacecraft-frame frequency ω' using

$$\omega = \omega' + \mathbf{k} \cdot \mathbf{V}_{\text{rel}} \tag{26}$$

where $\mathbf{V}_{\text{rel}}$ is the velocity of the spacecraft relative to the plasma frame; $\mathbf{V}_{\text{rel}}$ can be determined either from separate knowledge of the spacecraft trajectory or from spacecraft measurements of the mean electron and ion velocities in the spacecraft frame.

The validity of a calculation could be checked by verifying that $\mathbf{k}$ is an odd function of frequency and also that Faraday's law is satisfied in the spacecraft frame, i.e., that

$$\mathbf{k}(\omega) \times \mathbf{E}'(\omega) = \omega' \mathbf{B}(\omega) \tag{27}$$

where $\mathbf{E}'$ is the electric field measured in the spacecraft frame. Also, because $\mathbf{k}(\omega)$ is an odd function, equation (16) shows that $\langle \mathbf{J}(t) \times \mathbf{B}(t) \rangle = 0$ which is an easy condition to check.

4. Three Examples Using Synthetic Data

The validity of the method will now be demonstrated using examples of fields constructed from a synthetic data set. This data set is a time series defined over T discrete times $\{1, 2, 3, \ldots . T\}$ with vector potential

$$\mathbf{A}(\mathbf{x}, t) = \sum_{n=1}^{T/2} \left[\mathbf{A}_c(n) \cos(\mathbf{k}_n \cdot \mathbf{x} - \omega_n t) + \mathbf{A}_s(n) \sin(\mathbf{k}_n \cdot \mathbf{x} - \omega_n t) \right] \tag{28}$$

where

$$\omega_n = \frac{2n\pi}{T} \tag{29}$$

and

$$\mathbf{k}_n = \mathbf{k}_n(\omega_n). \tag{30}$$

The functional dependence given in equation (30) is completely arbitrary. Similarly, the values of $\mathbf{A}_c(n)$ and $\mathbf{A}_s(n)$ are completely arbitrary and are set by a random number generator in the synthetic data examples.

The magnetic field associated with the vector potential is $\mathbf{B} = \nabla \times \mathbf{A}$, so using equation (28),

$$\mathbf{B}(\mathbf{x}, t) = \sum_{n=1}^{T/2} \left[-\mathbf{k}_n \times \mathbf{A}_c(n) \sin(\mathbf{k}_n \cdot \mathbf{x} - \omega_n t) + \mathbf{k}_n \times \mathbf{A}_s(n) \cos(\mathbf{k}_n \cdot \mathbf{x} - \omega_n t) \right]. \tag{31}$$

Using a vector potential as the basic defining function means that the zero-divergence character of the magnetic field is automatically satisfied.

The electric current is given by Ampere's law $\mu_0 \mathbf{J} = \nabla \times \mathbf{A}$ so using equation (31),

$$\mu_0 \mathbf{J}(\mathbf{x}, t) = -\sum_{n=1}^{T/2} \left[\mathbf{k}_n \times \left(\mathbf{k}_n \times \mathbf{A}_c(n) \right) \cos(\mathbf{k}_n \cdot \mathbf{x} - \omega_n t) + \mathbf{k}_n \times \left(\mathbf{k}_n \times \mathbf{A}_s(n) \right) \sin(\mathbf{k}_n \cdot \mathbf{x} - \omega_n t) \right]. \tag{32}$$

The cross correlation of two functions $\psi(t)$ and $\chi(t)$ over the finite time series $\{1, 2, 3, \ldots, T\}$ is defined to be

$$C(\psi, \chi, \tau) = \frac{1}{T} \sum_{t=0}^{T-1} \psi(t) \chi(t') \tag{33}$$

where

$$t' = (t + \tau) \mod T. \tag{34}$$

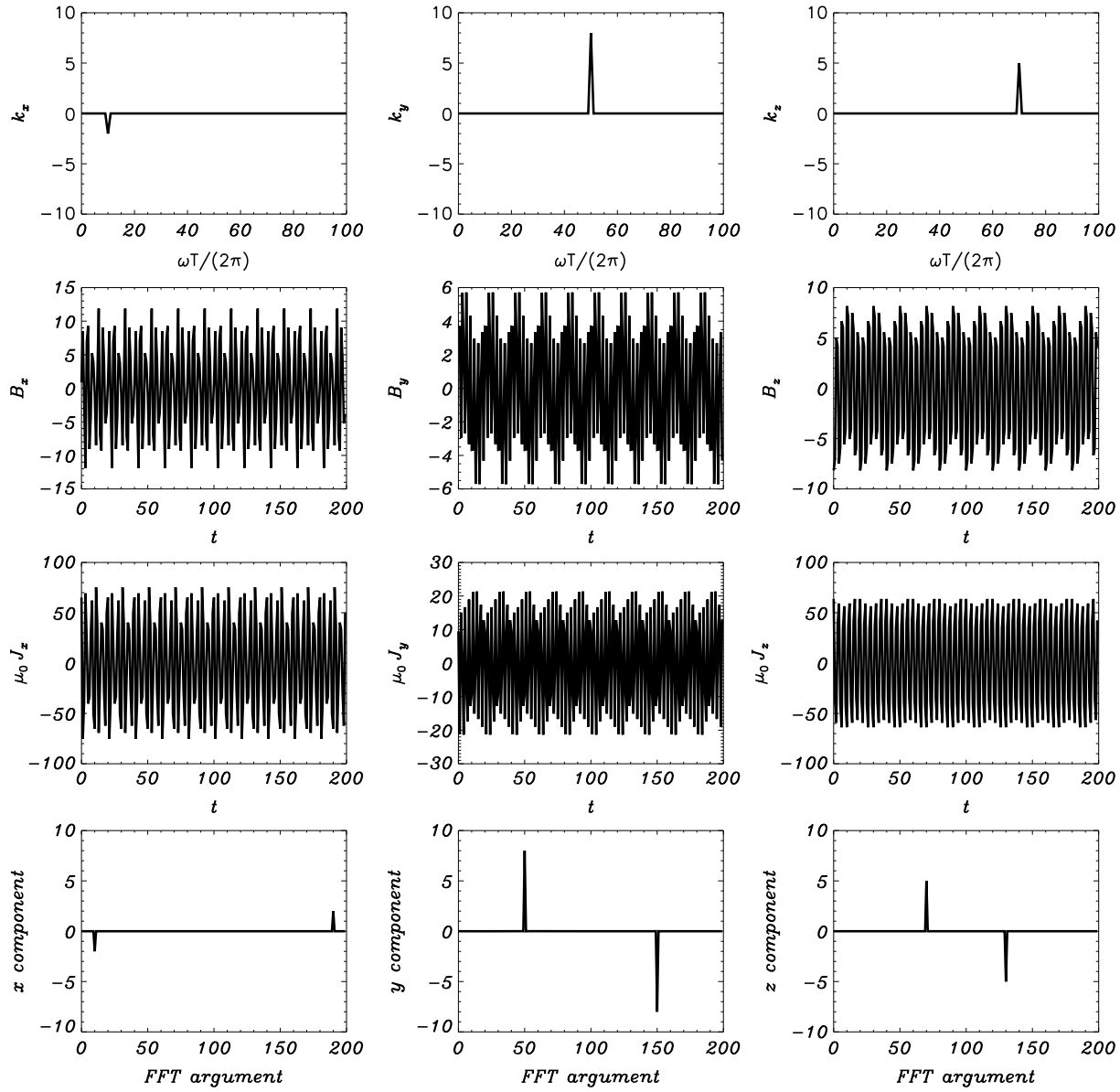

Figure 1. (first row) The $\mathbf{k}_n$ are prescribed as $k_x[10] = -2$, $k_y[50] = 8$, $k_z[70] = 5$ with all other $\mathbf{k}$ components set to zero. Each component of the $\mathbf{A}_c(n)$, $\mathbf{A}_s(n)$ is prescribed by a random number generator. (second row) B_x, B_y, and B_z . (third row) J_x, J_y, and J_z. (fourth row) The result calculated in equation (35). The exact correspondence between the fourth and first rows validates the method. The fourth row also shows, as predicted by equation (12), that $\mathbf{k}(-\omega) = -\mathbf{k}(\omega)$.

We define $\tilde{C}(\psi, \chi, \omega_n)$ as the discrete Fourier transform of $C(\psi, \chi, \tau)$, so equation (25) becomes

$$
\begin{aligned}
k_x(\omega_n) &= -\mu_0 \mathrm{Im} \frac{\tilde{C}(J_y, B_z, \omega_n) - \tilde{C}(J_z, B_y, \omega_n)}{\tilde{C}(B_x, B_x, \omega_n) + \tilde{C}(B_y, B_y, \omega_n) + \tilde{C}(B_z, B_z, \omega_n) + \varepsilon} \\
k_y(\omega_n) &= -\mu_0 \mathrm{Im} \frac{\tilde{C}(J_z, B_x, \omega_n) - \tilde{C}(J_x, B_z, \omega_n)}{\tilde{C}(B_x, B_x, \omega_n) + \tilde{C}(B_y, B_y, \omega_n) + \tilde{C}(B_z, B_z, \omega_n) + \varepsilon} \\
k_z(\omega_n) &= -\mu_0 \mathrm{Im} \frac{\tilde{C}(J_x, B_y, \omega_n) - \tilde{C}(J_y, B_x, \omega_n)}{\tilde{C}(B_x, B_x, \omega_n) + \tilde{C}(B_y, B_y, \omega_n) + \tilde{C}(B_z, B_z, \omega_n) + \varepsilon}
\end{aligned}
\tag{35}
$$

where the small quantity ε has been inserted to prevent having zero divided by zero for frequencies where there is no wave power.

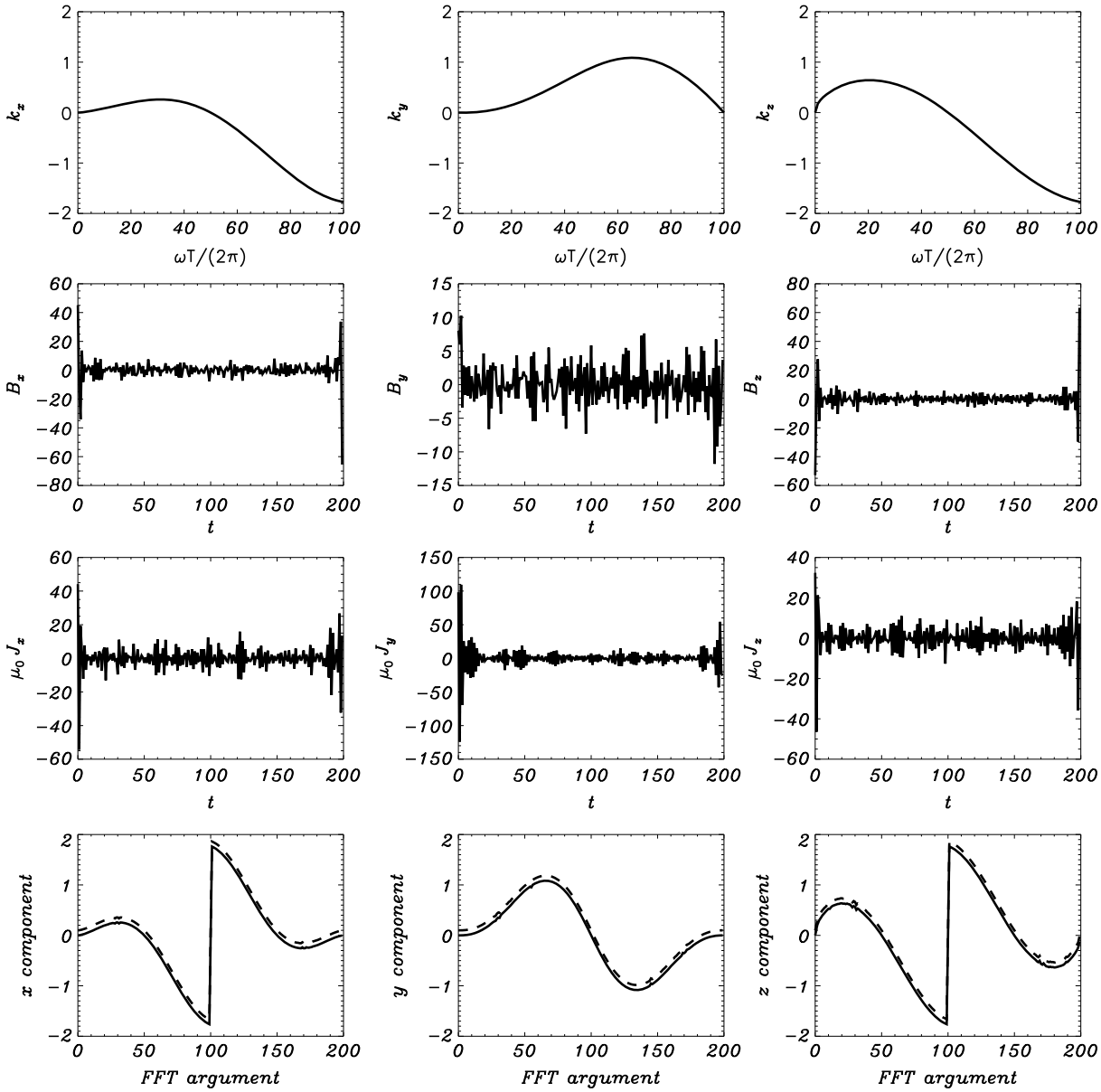

Figure 2. Same as Figure 1 except here the $\mathbf{k}_n$ are all finite and prescribed by a nontrivial functional dependence on ω. Because the $\mathbf{A}_c(n)$ and $\mathbf{A}_s(n)$ are prescribed by a random number generator, the magnetic field (second row) and the current (third row) have the appearance of random incoherent noise. Nevertheless, application of the procedure given in equation (35) recovers the prescribed $\mathbf{k}_n$ spectrum. The dashed line in the fourth row repeats the function prescribed in the top row with a slight vertical offset and shows that $\mathbf{k}_n$ calculated from the magnetic field and current using the proposed method recovers the prescribed $\mathbf{k}_n$.

Figures 1 and 2 plot examples of synthetic data calculated using an Interactive Data Language (IDL) code. In Figure 1, a few discrete values of $\mathbf{k}_n$ were prescribed, and the $6T$ vector coefficients $A_{c,x}(n), A_{c,y}(n), A_{c,z}(n), A_{s,x}(n), A_{s,y}(n), A_{s,z}(n)$ were each separately specified by a random number generator so as to generate the noisiest possible spectrum. In Figure 2 k_x, k_y, k_z were prescribed as continuous functions of ω_n.

The first rows of Figures 1 and 2 show the prescribed functional dependence of k_x, k_y, k_z on ω_n. The resulting $\mathbf{B}(\mathbf{x}, t)$ and $\mu_0\mathbf{J}(\mathbf{x}, t)$ computed using equations (31) and (32) are plotted in the second and third rows of Figures 1 and 2. The fourth rows of Figures 1 and 2 plot equation (35) where the Fourier transforms of the various correlation functions were calculated using the IDL fast Fourier transform. The odd parity of $\mathbf{k}$ predicted by equation (12) is evident, and it is seen that the calculated value of k_x, k_y, k_z is identical to the prescribed value.

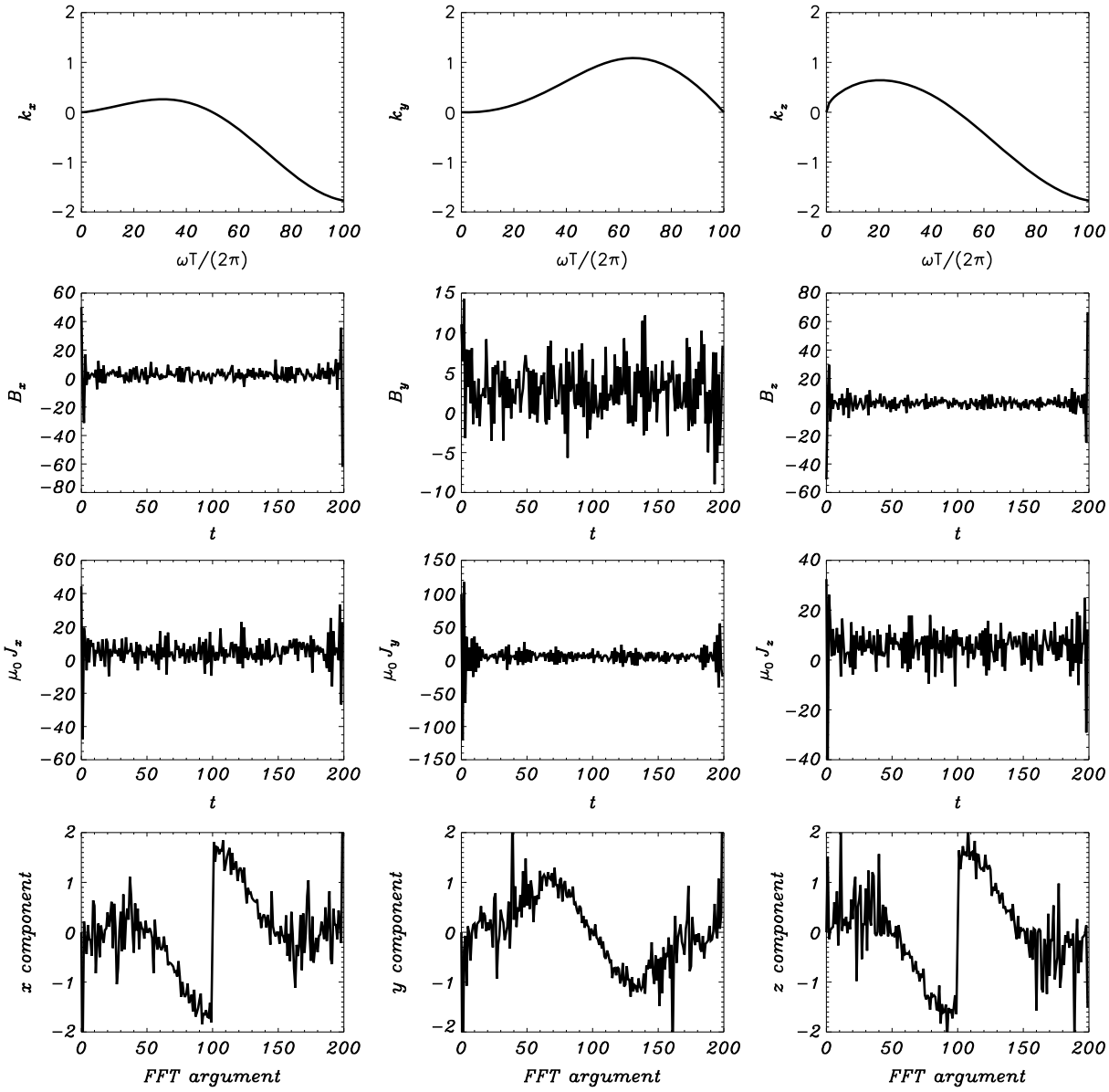

Figure 3. Same as Figure 2 except here noise has been added to both **J** and **B**; the noise amplitude is 50% of the RMS signal level for each of *J* and *B*. While noisy, the bottom row is similar to the bottom row of Figure 2.

In Figure 1, the values of components of the wave vector were set as follows: $k_x[10] = -2$, $k_y[50] = 8$, $k_z[70] = 5$ and all other k components set to zero while in Figure 2, the components were prescribed nontrivial functions of ω as plotted in Figures 1 and 2 (first row). The fourth rows of Figures 1 and 2 are identical to the respective top rows and since the top rows are the prescribed $\mathbf{k}(\omega)$, while the bottom rows are the values determined from equation (35) these examples validate the method for determining wave vector from measurements of the magnetic field and current at a single location.

To emphasize the validity of the results, Figure 2 also has the prescribed values of k_x, k_y, k_z plotted as dashed lines in the bottom row with a slight vertical offset; the solid lines (i.e., values of k_x, k_y, k_z as a function of frequency as predicted by equation (35)) are in exact agreement with the prescribed values. Because all $\mathbf{k}_n$ are used in Figure 2, because the $\mathbf{k}_n$ are dispersive, and because the $\mathbf{A}_c(n)$ and $\mathbf{A}_s(n)$ are prescribed by a random number generator, the magnetic field and current (second and third rows) have the appearance of random noise. Nevertheless, the procedure still recovers the prescribed dependence of **k** on frequency.

An actual spacecraft measurement will have noise in both the current and magnetic field detectors. However, there cannot be any noise in the actual physical current density and physical magnetic field because these fields are related to each other by equation (6). To see how detector noise affects the measurement, a noise signal having amplitude equal to 50% of the RMS magnetic fluctuation amplitude has been added to both the current and magnetic field signals used for Figure 2. This noisy situation is shown in Figure 3, and it is seen that the fourth row of Figure 3 is a noisy version of the fourth row of Figure 2. If the added noise amplitude is much smaller than 50% of the signal amplitudes, then the bottom row of the resulting figure (not shown) reverts to the fourth row of Figure 2, while if the added noise is much larger than 50%, the bottom row of the resulting figure (not shown) becomes extremely noisy and bears no resemblance to the fourth row of Figure 2. This shows that the **k** measurement technique works well provided the detector noise is small compared to the signal RMS amplitude for both **J** and **B**.

The IDL code used to produce Figures 1–3 is provided in the supporting information. This code has been written so it can be easily modified to work with magnetic field and current data from an externally supplied file.

5. Determination of $\mathbf{A}_c(n)$ and the $\mathbf{A}_s(n)$

Once the $\mathbf{k}_n$ have been determined, it is then possible to determine the $\mathbf{A}_c(n)$ and the $\mathbf{A}_s(n)$ in which case the magnetic field and current could be calculated at arbitrary locations using equations (31) and (32). It is necessary to first change to Coulomb gauge. We therefore define $\mathbf{A}' = \mathbf{A} - \nabla\psi$ where ψ is chosen so that $\nabla^2\psi = \nabla\cdot\mathbf{A}$ in which case for each frequency component n it is seen that

$$-\mathbf{k}_n\cdot\mathbf{k}_n\psi_c(n) = i\mathbf{k}_n\cdot\mathbf{A}_c(n) \tag{36}$$

and similarly for the sine component. Equation (36) gives $\psi_c(n) = -i\mathbf{k}_n\cdot\mathbf{A}_c(n)/\left(\mathbf{k}_n\cdot\mathbf{k}_n\right)$ so the Coulomb-gauge vector potential would have cosine and sine frequency components:

$$\begin{aligned}\mathbf{A}'_c(n) &= \mathbf{A}_c(n) - \mathbf{k}_n\frac{\mathbf{k}_n\cdot\mathbf{A}_c(n)}{\mathbf{k}_n\cdot\mathbf{k}_n}\\ \mathbf{A}'_s(n) &= \mathbf{A}_s(n) - \mathbf{k}_n\frac{\mathbf{k}_n\cdot\mathbf{A}_s(n)}{\mathbf{k}_n\cdot\mathbf{k}_n}.\end{aligned} \tag{37}$$

These satisfy $i\mathbf{k}_n\cdot\mathbf{A}'_{c,s}(n) = 0$.

Because $\nabla\times\mathbf{A} = \nabla\times\mathbf{A}'$, equation (32) could be expressed using the Coulomb gauge vector potential as

$$\mu_0\mathbf{J}(\mathbf{x},t) = -\sum_{n=1}^{T/2}\left[\mathbf{k}_n\times\left(\mathbf{k}_n\times\mathbf{A}'_c(n)\right)\cos(\mathbf{k}_n\cdot\mathbf{x}-\omega_n t) + \mathbf{k}_n\times\left(\mathbf{k}_n\times\mathbf{A}'_s(n)\right)\sin(\mathbf{k}_n\cdot\mathbf{x}-\omega_n t)\right]. \tag{38}$$

However, because $\mathbf{k}_n\times\left(\mathbf{k}_n\times\mathbf{A}'_c(n)\right) = -k_n^2\mathbf{A}'_c(n)$, equation (38) reduces at $\mathbf{x} = 0$ to

$$\mu_0\mathbf{J}(0,t) = \sum_{n=1}^{T/2}\left[k_n^2\mathbf{A}'_c(n)\cos(\omega_n t) - k_n^2\mathbf{A}'_s(n)\sin(\omega_n t)\right]. \tag{39}$$

The Fourier transform of equation (39) gives

$$\begin{aligned}\mathbf{A}'_c(n) &= \frac{2\mu_0}{Tk_n^2}\sum_{t=0}^{T}\mathbf{J}(0,t)\cos(\omega_n t)\\ \mathbf{A}'_s(n) &= -\frac{2\mu_0}{Tk_n^2}\sum_{t=0}^{T}\mathbf{J}(0,t)\sin(\omega_n t).\end{aligned} \tag{40}$$

Because the $\mathbf{k}_n$ have been determined by equation (35), the coefficients $\mathbf{A}'_c(n)$ and $\mathbf{A}'_s(n)$ are now fully determined in which case the magnetic field and current at arbitrary locations and time can be calculated using equations (31) and (32). If the wave is dispersive, this calculation could be used to find the location where all frequency components are in phase with each other. If such a location exists, then it would correspond to the location of a pulsed source (e.g., localized reconnection) generating the dispersive waves.

6. Requirement That There be a Unique Wave Vector for Each Frequency

The method presumes that there is a unique wave vector $\mathbf{k}$ for each frequency, i.e., $\mathbf{k} = \mathbf{k}(\omega)$. Because $\mathbf{k}$ is a vector while ω is a scalar, a dispersion relation typically does not require this unique mapping; the most obvious example being the situation where both $\mathbf{k}$ and $-\mathbf{k}$ satisfy the dispersion relation $\omega^2 = k^2 v_A^2$ where v_A is the Alfvén velocity. If it happened that two different wave vectors $\mathbf{k}_1 \neq \mathbf{k}_2$ were associated with the same frequency at the measurement location, so

$$\mathbf{B}(\omega, \mathbf{x}) = \mathbf{B}_1(\omega) e^{i\mathbf{k}_1(\omega)\cdot\mathbf{x}} + \mathbf{B}_2(\omega) e^{i\mathbf{k}_2(\omega)\cdot\mathbf{x}} \tag{41}$$

then at the measurement location $\mathbf{x} = 0$ equation (6) would be replaced by

$$\mu_0 \mathbf{J}(\omega) = i\mathbf{k}_1(\omega) \times \mathbf{B}_1(\omega) + i\mathbf{k}_2(\omega) \times \mathbf{B}_2(\omega). \tag{42}$$

Thus, equation (7) would be replaced by

$$\begin{aligned} \mu_0 \mathbf{J}(\omega) \times \mathbf{B}^*(\omega) &= \left[i\mathbf{k}_1(\omega) \times \mathbf{B}_1(\omega) + i\mathbf{k}_2(\omega) \times \mathbf{B}_2(\omega)\right] \times \left[\mathbf{B}_1^*(\omega) + \mathbf{B}_2^*(\omega)\right] \\ &= -i\mathbf{k}_1 \left|B_1\right|^2 - i\mathbf{k}_2 \left|B_2\right|^2 + \mathbf{B}_1 i\mathbf{k}_1 \cdot \mathbf{B}_2^* - i\mathbf{k}_1 \mathbf{B}_1 \cdot \mathbf{B}_2^* + \mathbf{B}_2 i\mathbf{k}_2 \cdot \mathbf{B}_1^* - i\mathbf{k}_2 \mathbf{B}_2 \cdot \mathbf{B}_1^* \end{aligned} \tag{43}$$

which unlike equation (7) provides insufficient information to solve for $\mathbf{k}_1$ or $\mathbf{k}_2$. An obvious special case of this problem would be measurement done at the magnetic node of a standing wave [*Takahashi et al.*, 2010] for a frequency ω since in this case $\mathbf{k}_1 = -\mathbf{k}_2$ and $\mathbf{B}_1(\omega) = -\mathbf{B}_2(\omega)$ so $\mathbf{B} = 0$ causing the denominator in equation (25) to vanish.

A check that the waves at a given frequency ω consist of a single plane wave as presumed in equations (4)–(6) and not as a sum of two or more different $\mathbf{k}$ vectors as shown in equations (41) and (42) would be to follow through the procedure given here in equations (8) and its equivalent, equation (35) to calculate a wave vector $\mathbf{k}$. If there is a single plane wave, then this calculated $\mathbf{k}$ should be the unique wave vector associated with the frequency ω in which case this $\mathbf{k}$ will satisfy equations (6) for the measured $\mathbf{J}(\omega)$ and $\mathbf{B}(\omega)$. However, if there are multiple $\mathbf{k}$'*s* for the given frequency, then clearly, the single $\mathbf{k}$ calculated using equation (8) and its equivalent, equation (35), will not work in equation (6). A quantitative metric is thus the following: for each frequency construct a wave vector $\mathbf{k}_{calc}$ from equation (35) and use this to predict a current $\mu_0 \mathbf{J}_{pred} = i\mathbf{k}_{calc} \times \mathbf{B}_{meas}$ where $\mathbf{B}_{meas}$ is the measured magnetic field. Then calculate the error angle between $\mathbf{J}_{pred}$ and the measured current $\mathbf{J}_{meas}$ where this error angle is defined as $\theta_{error} = \cos^{-1}(\mathbf{J}_{pred} \cdot \mathbf{J}_{meas} / (\left|\mathbf{J}_{pred}\right| \left|\mathbf{J}_{meas}\right|)$ and calculate the relative magnitude error $M_{error} = \left|\left(\left|\mathbf{J}_{pred}\right| - \left|\mathbf{J}_{meas}\right|\right)\right| / \left(\left|\mathbf{J}_{pred}\right| + \left|\mathbf{J}_{meas}\right|\right)$. If there is a single plane wave, then $\mathbf{J}_{pred}$, and $\mathbf{J}_{meas}$ will be identical so both θ_{error} and M_{error} will be zero, but if there are multiple plane waves at the frequency under consideration, the errors will be large. This requirement of a single plane wave also applies to *Balikhin et al.* [2003] and to any other method that assumes a single plane wave for each frequency and uses phase measurements to determine the unique wave vector.

Besides standing waves, another situation where this ambiguity could occur would be where two spatially distinct sources emit waves at the same frequency. The $\mathbf{k}$ vector would have some specific orientation relative to each source, and so the two sources would provide two different $\mathbf{k}$ vectors. As an analogy, consider a pebble dropped at the origin of a pond so concentric periodic ripples are formed. An observer on the *x* axis would see finite k_x at a frequency ω, while an observer on the *y* axis would see finite k_y at the same ω so there is a unique mapping from ω to $\mathbf{k}$ for each observer. However, if pebbles were dropped into the pond at two locations, then an observer might be on the *x* axis of one pebble and the *y* axis of the other and so would see both k_x and k_y so there would not be a unique $\mathbf{k}$ for each ω. If the signal comes from a single source (e.g., a localized reconnection event like a single pebble dropped in a pond), it is likely that there will be a unique $\mathbf{k}$ for each ω component observed at the spacecraft. For example, the assumption that $\mathbf{k} = \mathbf{k}(\omega)$ was used in equation (35) and Figure 8 of *Narita et al.* [2010].

The Doppler shift given in equation (26) also affects the extent to which wave vectors are unique. Two cases are of interest. In the first case, suppose that a standing wave exists at a frequency ω_1 in the lab frame so there are two waves, the first wave with wave vector $\mathbf{k}_1$ and the second wave with wave vector $-\mathbf{k}_1$ so a typical magnetic field varies as $\cos(\mathbf{k}_1 \cdot \mathbf{x} - \omega_1 t) + \cos(-\mathbf{k}_1 \cdot \mathbf{x} - \omega_1 t) = 2\cos\left(\mathbf{k}_1 \cdot \mathbf{x}\right)\cos(\omega_1 t)$. A spacecraft located at a node, i.e., where $\cos\left(\mathbf{k}_1 \cdot \mathbf{x}\right) = 0$, would see no magnetic field at frequency ω_1 and so would not be able to deduce a wave vector. However, a spacecraft moving with a velocity $\mathbf{V}_{rel}$ would see the first wave at a spacecraft frame

frequency $\omega' = \omega_1 - \mathbf{k}_1 \cdot \mathbf{V}_{rel}$ and the second wave at a frequency $\omega' = \omega_1 + \mathbf{k}_1 \cdot \mathbf{V}_{rel}$ so the lab frame frequency degeneracy would not exist in the spacecraft frame in which case there would be a unique $\mathbf{k}$ associated with each frequency. Standing waves develop when there is reflection at the walls of a cavity. While cavities exist in some space situations, very often the system is open so waves propagate without reflection and there are no standing waves.

Yet another possibility for ambiguity consists of two distinct traveling waves with frequencies ω_1 and ω_2 in the lab frame with respective wave vectors $\mathbf{k}_1$ and $\mathbf{k}_2$. The spacecraft would see frequencies $\omega_1' = \omega_1 + \mathbf{k}_1 \cdot \mathbf{V}_{rel}$ and $\omega_2' = \omega_2 + \mathbf{k}_2 \cdot \mathbf{V}_{rel}$ in its frame so if it turns out that $\omega_1' = \omega_2'$ then the frequency $\omega' = \omega_1' = \omega_2'$ would be associated with the two different wave vectors $\mathbf{k}_1$ and $\mathbf{k}_2$ and there would not be a unique wave vector associated with the frequency ω'. This situation corresponds to $\omega_2 - \omega_1 = (\mathbf{k}_2 - \mathbf{k}_1) \cdot \mathbf{V}_{rel}$. If the lab frame frequencies and wave vectors are nearly the same so $\omega_2 = \omega_1 + \delta\omega$ and $\mathbf{k}_2 = \mathbf{k}_1 + \delta\mathbf{k}$, then $\delta\omega = \delta\mathbf{k} \cdot \mathbf{V}_{rel}$ so $\mathbf{V}_{rel} = \partial\omega/\partial\mathbf{k}$, i.e., the spacecraft velocity is at the group velocity. This is reasonable since a pulse travels at the group velocity, and if the spacecraft traveled at the same velocity as the pulse, then the pulse would appear stationary in time so there would be no time-dependent signal in the spacecraft frame.

7. Summary

A method has been presented showing that the magnitude and direction of the wave vector $\mathbf{k}(\omega)$ can be determined from single-spacecraft measurements of the time-dependent current and magnetic field provided that these fields are produced by quasi-neutral traveling waves and there is a unique mapping from frequency to wave vector. Using $\mathbf{k}(\omega)$ together with knowledge of the spacecraft velocity relative to the plasma frame, the plasma-frame frequency of the waves can be established. Examples constructed from synthetic data verify the method and also indicate the feasibility of reconstructing the complete space-time dependence of the electric and magnetic fields from measurements made at a single location.

Acknowledgments
This material is based upon work supported by the U.S. Department of Energy Office of Science, Office of Fusion Energy Sciences under award DE-FG02-04ER54755 and DE-SC0010471, by the National Science Foundation under award 1348393, and by the Air Force Office of Scientific Research under award FA9550-11-1-0184. The author would like to thank A.F. Viñas for useful comments. This manuscript does not use any experimental data.

References

Balikhin, M. A., O. A. Pokhotelov, S. N. Walker, E. Amata, M. Andre, M. Dunlop, and H. S. C. K. Alleyne (2003), Minimum variance free wave identification: Application to Cluster electric field data in the magnetosheath, *Geophys. Res. Letters*, *30*, 1508.

Bellan, P. M. (2008), *Fundamentals of Plasma Physics*, Eq.14.24, Cambridge Univ. Press, Cambridge.

Bellan, P. M. (2012), Improved basis set for low frequency waves, *J. Geophys. Res.*, *117*, A12219, doi:10.1029/2012JA017856.

Bernstein, I. B., and F. Engelmann (1966), Quasi-linear theory of plasma waves, Eq.20, *Phys. Fluids*, *9*(5), 937–952.

Hobara, Y., S. N. Walker, M. Balikhin, O. A. Pokhotelov, M. Dunlop, H. Nilsson, and H. Reme (2007), Characteristics of terrestrial foreshock ULF waves: Cluster observations, *J. Geophys. Res.*, *112*(A7), A07202, doi:10.1029/2006JA012142.

Korepanov, V., and F. Dudkin (1999), Comparative analyiss of current density meters operating in space plasmas, *Adv. Space Res.*, *23*, 1541–1544.

Motschmann, U., and K.-H. Glassmeier (1998), Multi-spacecraft filtering: Plasma mode recognition, in *Analysis Methods for Multi-Spacecraft Data*, edited by G. Paschmann and P. W. Daly, chap. 4, 79–89, ISSI/ESA, Berne.

Narita, Y., K.-H. Glassmeier, and U. Motschmann (2010), Wave vector analyis methods using multi-point measurements, *Nonlinear Processes Geophys.*, *17*, 383–394.

Santolik, O., M. Parrot, and F. Lefeuvre (2003), Singular value decomposition methods for wave propagation analysis, *Radio Sci.*, *38*(1), 1010.

Schmidt, G. (1979), *Physics of High Temperature Plasmas*, Section 9.3, Academic Press, New York.

Sonnerup, B. U., and M. Scheible (1998), Minimum and maximum variance analysis, in *Analysis Methods for Multi-Spacecraft Data*, edited by G. Paschmann and P. W. Daly, chap. 8, 185–220, ISSI/ESA, Bern.

Takahashi, K., et al. (2010), Multipoint observation of fast mode waves trapped in the dayside plasmasphere, *J. Geophys. Res.*, *115*, A12247, doi:10.1029/2010JA015956.

Volwerk, M., T. L. Zhang, K. H. Glassmeier, A. Runov, W. Baumjohann, A. Balogh, H. Reme, B. Klecker, and C. Carr (2008), Study of waves in the magnetotail region with Cluster and DSP, *Adv. Space Res.*, *41*(10), 1593–1597.

Walker, S. N., M. A. Balikhin, D. R. Shklyar, K. H. Yearby, P. Canu, C. M. Carr, and I. Dandouras (2015), Experimental determination of the dispersion relation of magnetosonic waves, *J. Geophys. Res. Space Physics*, *120*(11), 9632–9650.